# Metal peroxides for cancer treatment

Jin He [a,1], Lian-Hua Fu [a,1], Chao Qi [b], Jing Lin [a], Peng Huang [a,*]

[a] *Marshall Laboratory of Biomedical Engineering, International Cancer Center, Laboratory of Evolutionary Theranostics (LET), School of Biomedical Engineering, Health Science Center, Shenzhen University, Shenzhen, 518060, China*
[b] *Key Laboratory of Biorheological Science and Technology, Ministry of Education, College of Bioengineering, Chongqing University, Chongqing, 400044, China*

A B S T R A C T

In recent years, metal peroxide ($MO_2$) such as $CaO_2$ has received more and more attention in cancer treatment. $MO_2$ is readily decompose to release metal ions and hydrogen peroxide in the acidic tumor microenvironment (TME), resulting metal ions overloading, decreased acidity and elevated oxidative stress in TME. All of these changes making $MO_2$ an excellent tumor therapeutic agent. Moreover, by combining $MO_2$ with photosensitizers, enzymes or Fenton reagents, $MO_2$ can assist and promote various tumor therapies such as photodynamic therapy and chemodynamic therapy. In this review, the synthesis and modification methods of $MO_2$ are introduced, and the representative studies of $MO_2$-based tumor monotherapy and combination therapy are discussed in detail. Finally, the current challenges and prospects of $MO_2$ in the field of tumor therapy are emphasized to promote the development of $MO_2$-based cancer treatment.

## 1. Introduction

Cancer has always been one of the most threatening diseases for human survival. In the past ten years, the incidence of malignant tumors in China has maintained an annual increase of about 3.9%, even worse, estimated 9.6 million died of cancer worldwide in 2018 [1,2]. Therefore, the development of cancer therapeutic methods to fight against cancer is urgely needed.

With the progress of science and technology, in addition to traditional chemotherapy and radiotherapy, scientists have already developed various novel cancer therapies, including photodynamic therapy (PDT), chemodynamic therapy (CDT), photothermal therapy and so on [3–5]. However, the rapid proliferation of cancer cells resulted the supply and consumption of oxygen ($O_2$) unbalanced, combined with the abnormal structure and function of tumor blood vessels, made hypoxia the most prominent feature of tumor microenvironment (TME) [6,7]. As a result, many therapeutic resistance effects will occur. For example, insufficient $O_2$ sources lead to low reactive oxygen species (ROS) production and decrease cell sensitivity to ROS, which greatly reduce the effectiveness of $O_2$-dependent therapies such as PDT and radiation therapy [8,9]. Moreover, some chemotherapeutic drugs also failed to be activated in a hypoxic TME. Therefore, it is necessary to regulate the hypoxic TME to improve the antitumor effect.

To cope with the challenge of tumor hypoxia, the hyperbaric oxygen (HBO) therapy in which patients breathe pure $O_2$ or high-concentration $O_2$ in a hyperbaric chamber can used as an adjuvant therapy. HBO therapy is beneficial to increase the partial pressure of $O_2$ in the plasma and promote the $O_2$ transport to hypoxic tumor tissue [10]. However, HBO therapy has many side effects such as $O_2$ poisoning, barotrauma and decompression sickness [11]. The method by employing catalase (CAT) or $MnO_2$ to convert the intracellular hydrogen peroxide ($H_2O_2$) to $O_2$ has also been applied to overcome the hypoxia [12–14]. However, the $O_2$ supplied by $MnO_2$ degradation and CAT catalysis also face to be exhausted due to the limited intratumoral $H_2O_2$. Fortunately, metal peroxides ($MO_2$) has been explored better to alleviate hypoxia by a disproportionation reaction with $H_2O$ in tumor tissue.

$MO_2$, including $CaO_2$, $CuO_2$, $MgO_2$, $BaO_2$, $ZnO_2$ etc., can be considered as the product of two hydrogen atoms in $H_2O_2$ replaced by metal ions. $MO_2$ can cause strong oxidation effect by its decomposition products (such as $H_2O_2$) under acidic condition, while it can also slowly release $O_2$ in water or under heating conditions [15]. These properties making it widely used in antibacterial [16], agricultural production [17], environmental protection [18], and other aspects [19]. Many of its other properties, if exploited, can also provide new ideas for cancer

---

therapy: (I) Under acidic conditions, $MO_2$ can react with $H_2O$ to produce $H_2O_2$, which causes increased oxidative stress; (II) The generated $H_2O_2$ reacts with Fenton or Fenton-like reagents (such as $Fe^{2+}$, $Mn^{2+}$, $Cu^+$, $Co^{2+}$, etc.) to produce hydroxyl radical ($^.OH$) and realize CDT; (III) The produced $H_2O_2$ can be decomposed by CAT or $MnO_2$ to produce $O_2$ and increase the efficacy of $O_2$-dependent cancer therapies such as PDT and radiation therapy; (IV) The released metal ions have some unexpected effects, for instance, calcium overloading caused by $Ca^{2+}$ ions that released from $CaO_2$ makes mitochondria damage [20]; while the $Ba^{2+}$ ions generated by the disproportionation reaction of $BaO_2$ act as a potassium ion channel inhibitor to inhibit tumor cell proliferation [21]. The application of $MO_2$ in cancer treatment is developed fastly, and there is no doubt that $MO_2$ is a promising candidate to regulate TME for various treatments.

In this review, recent advances in the preparation and application of $MO_2$ in cancer therapy will be discussed. As shown in Scheme 1, we starting from the preparation and surface modification of $MO_2$, and then elaborate the design ideas and application examples of $MO_2$ in CDT, PDT, ion interference therapy and various types of synergistic therapy. Finally, the current challenges and prospects of $MO_2$-based cancer treatment will be presented.

## 2. Synthesis and surface modification of $MO_2$

To date, several preparation methods of $MO_2$ are developed, including hydrolyzation-precipitation method [22,23], underwater Leidenfrost dynamic chemistry method [24], reversed-phase microemulsion method [25], gas diffusion method [26], and sonochemical method [27]. Due to the instability of $MO_2$, some surface modification is necessary to achieve better applications in biomedical fields, frequently used surface modifiers are polyethylene glycol (PEG), polyvinyl pyrrolidone (PVP), CO-520, and hyaluronic acid (HA) [23,25,28,29]. Proper surface modification not only increases the stability of $MO_2$, but also improves the dispersion of nanoparticles (NPs), even be possible to target the tumor. The preparation and surface modification of $MO_2$ are summarized in Table 1, and will be discussed in detail in this section.

### 2.1. Hydrolyzation-precipitation method

Currently, the hydrolyzation-precipitation method is the most widely used method to prepare $MO_2$. This method usually used metal

chloride, metal acetate or metal carbonate as precursors, through adding $H_2O_2$ to the alkaline aqueous solution of metal salt to precipitating the water-insoluble $MO_2$. This method has the advantages of simple, mild conditions, low cost, and the size of NPs can be adjusted to several nanometers for the further construction of nanostructures.

Take the synthesis of $CaO_2$ for example, the $CaO_2$ hydrate was obtained by Eq. (1), and then the reaction was promoted to precipitate in favor of the metal peroxide by adding ammonia to neutralize the HCl, Eq. (2) [40].

$$CaCl_2 + H_2O_2 \rightarrow CaO_2 \text{ (hydrate)} + 2HCl \tag{1}$$

$$2HCl + 2NH_3 \rightarrow 2NH_4Cl \tag{2}$$

Based on the above theory, Xia et al. reported an approach to synthesize $CaO_2$ nanocrystals and their spherical aggregates [41]. They chose ethanol as the solvent to reduce the hydrolysis of $CaO_2$ NPs. Typically, 2–15 nm primary nanocrystals were obtained through adding $H_2O_2$ into an ethanol solution with $CaCl_2$ and PVP, in which PVP cooperated with $Ca^{2+}$ to affect the growth and assembly of the nanocrystalline, resulting in spherical aggregates of polycrystalline structure with uniform size (Fig. 1). Therefore, the size of NPs can be easily controlled by adjusting the concentration of $CaCl_2$ and/or PVP. The prepared $CaO_2$ could greatly improve the antibacterial activity by releasing $H_2O_2$ and $O_2$ at a faster rate after contact with $H_2O$, which provided a new way for $CaO_2$ to be used as a nano-drug. It is worth mentioning that PVP not only regulates particle size as mentioned above, but also acts as a stabilizer in hydrolyzed precipitation. Similarly, PEG can also be used as a stabilizer to modify the surface of $MO_2$ [22,33, 37,38].

Bu et al. reported the synthesis of $BaO_2$ by hydrolysis and precipitation reaction [21]. In short, sodium formate and $BaCl_2$ aqueous solution were mixed with ultrasonic and then added to anhydrous methanol. Excessive amounts of $H_2O_2$ were dropped into the mixture after vigorously stirring, choline hydroxide aqueous solution was followed to precipitate the $BaO_2$ NPs (Fig. 2A). They pointed out that the selection of organic ligands has a great influence on the growth rate and orientation of $BaO_2$ nanocrystal, so products of different particle sizes and morphology will be obtained. In their study, $BaO_2$ particle with sub-micron scale can be obtained by using free $Ba^{2+}$ as the precursor, while $BaO_2$ nanocrystal with bamboo-structure will be formed by using formate coordinated $Ba^{2+}$ as the precursor. The authors made a variety of attempts and found that the stronger the coordination ability with $Ba^{2+}$, the smaller products will be obtained (Fig. 2B). Therefore, the introduction of a ligand with a certain coordination ability with $Ba^{2+}$ into the reaction can effectively limit the growth of the crystal to get nanosized $BaO_2$ particles. Shape controllability gives nanomaterials different specific surface areas and functions, which is an important link in the construction of nanomaterials theranostics platform.

In the example above, the authors modified $BaO_2$ with a biodegradable strong chelating agent *L*-glutamic acid (*N*-diacetic acid) to reduce the damage of free $Ba^{2+}$ to normal tissues. When drugs entered the tumor, X-ray stimulation could separate $Ba^{2+}$ and chelating agent, promoting the treatment of tumor. Which proved that $MO_2$ can be modified by chelating method and enhanced the performance of $MO_2$ performance.

In addition, hyaluronic acid (HA), sodium hyaluronate (SH), and tannic acid (TA) are also used for surface modification of $MO_2$. For example, after stabilization by HA, $CaO_2$ can remain stable in the humoral environment, and can only be degraded in the acidic TME to achieve material stabilization and tumor targeting [20,29,36]. To sum up, proper surface modification not only increases the stability of $MO_2$, but also improves the dispersion of NPs, even be possible to target tumor.
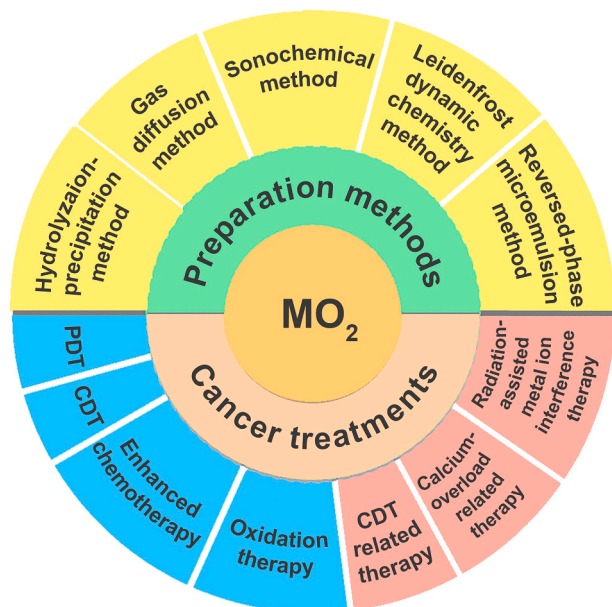


**Scheme 1.** Preparations and applications of $MO_2$ in tumor therapy.

**Table 1**
The synthesis, surface modification and applications of $MO_2$-based biomaterials.

| $MO_2$ | Preparation | Morphology and size | Surface modifier | Applications | Ref. |
|---|---|---|---|---|---|
| $CaO_2$ | Hydrolyzation-precipitation method | Particle, <5 nm | SH | Calcium-overload/Oxidation therapy | [20] |
| $CaO_2$ | Hydrolyzation-precipitation method | Particle, $15 \pm 10$ nm | PEG-200 | PDT | [22] |
| $CaO_2$ | Hydrolyzation-precipitation method | Spherical structure, 5–15 nm | PEG-200 | PDT | [23] |
| $CaO_2$ | Hydrolyzation-precipitation method | Particle | PVP | PDT | [28] |
| $CaO_2$ | Hydrolyzation-precipitation method | Particle, $107 \pm 11$ nm | HA | CDT | [29] |
| $CaO_2$ | Hydrolyzation-precipitation method | Clusters, $300 \pm 20$ nm | PEG-200 | PDT | [30] |
| $CaO_2$ | Hydrolyzation-precipitation method | Spherical structure, $116.0 \pm 7.6$ nm | PEG-200 | PDT | [31] |
| $CaO_2$ | Hydrolyzation-precipitation method | Particle, < 200 nm | PEG-200 | Chemotherapy/CDT | [15] |
| $CaO_2$ | Hydrolyzation-precipitation method | Particle, 20–30 nm | PEG-200 | Magnetic hyperthermia therapy/CDT | [32] |
| $CaO_2$ | Hydrolyzation-precipitation method | Particle, ~20 nm | PEG-400 | CDT/PDT | [33] |
| $CaO_2$ | Hydrolyzation-precipitation method | Particle, ~18 nm | PEG-200 | PTT/CDT | [34] |
| $CaO_2$ | Hydrolyzation-precipitation method | Particle, ~8 nm | PVP | PTT/CDT | [35] |
| $CaO_2$ | Hydrolyzation-precipitation method | Particle, 200–240 nm | TA | – | [36] |
| $CaO_2$ | Gas diffusion method | Spherical structure, 90 nm | $SiO_2$ | Immunochemotherapy | [26] |
| $CaO_2$ | Reversed-phase microemulsion method | Particle, $273.4 \pm 7.8$ nm | CO-520 | Chemotherapy | [25] |
| $CuO_2$ | Hydrolyzation-precipitation method | Nanodots, ~16.3 nm | PVP | CDT | [37] |
| $ZnO_2$ | Hydrolyzation-precipitation method | Particle, 66.1 nm | PVP | Oxidation therapy | [38] |
| $ZnO_2$ | Leidenfrost dynamic chemistry method | Particle, size-tailored | – | Oxidation therapy | [24] |
| $ZnO_2$ | Sonochemical method | Particle | – | – | [27] |
| $MgO_2$ | Reversed-phase microemulsion method | Nanosheets, 100–200 nm | CO-520 | Molecular dynamic therapy | [39] |
| $BaO_2$ | Hydrolyzation-precipitation method | Bamboo-structure, <15 nm | GLDA | Radiation-assisted metal ion interference therapy | [21] |

Notes: PEG, polyethylene glycol; HA, hyaluronic acid; SH, sodium hyaluronate; PVP, polyvinyl pyrrolidone; TA, tannic acid; GLDA, *N, N*-bis(carboxymethyl)-L-glutamic acid tetrasodium salt.
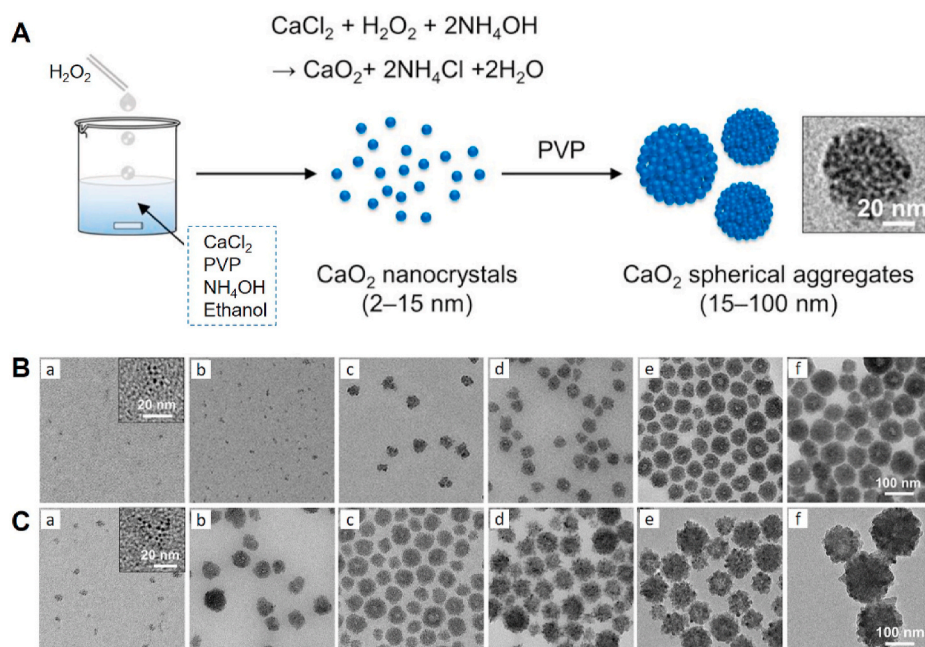


**Fig. 1.** (A) Schematic illustration of the formation of spherical aggregates through PVP-directed aggregation of $CaO_2$ primary nanocrystals. (B) TEM images of $CaO_2$ spherical aggregates synthesized in the presence of $CaCl_2$ at different concentrations: a) 2.1, b) 4.2, c) 8.4, d) 25.2, e) 42, and f) 168 mM, respectively. (C) TEM images of $CaO_2$ spherical aggregates synthesized in the presence of PVP at different concentrations: a) 43.2, b) 30.9, c) 21.6, d) 6.17, e) 1.23, and f) 0 mg mL$^{-1}$, respectively. Reproduced with permission from Ref. [41]. Copyright 2019, Wiley-VCH.

### 2.2. Leidenfrost dynamic chemistry method

As we all known, a drop of water on an iron plate at 100 °C will boil and evaporate quickly. But if the temperature of the iron continues to rise, the water droplets will roll around the iron plate and evaporate at a slower rate. Leidenfrost first found and put forward the phenomenon in 1756, and pointed out that when the iron temperature reached the Leidenfrost point, water droplets in contact with the iron part will quickly form a steam, other part will remain liquid, due to the heat transfer of vapor is much slower than liquid water. Vapor layer can form a protective layer to avoid liquid water contact with the iron plate directly, so as to reduce the evaporation rate of the water. This phenomenon is well known Leidenfrost phenomenon [42,43].

Inspired by the volcano-induced dynamic chemistry of the deep sea [44], Moheb Abdelaziz and co-authors found that Leidenfrost can occur underwater. By virtue of the research of underwater Leidenfrost phenomenon, they designed a new tool for customized creation of nanoclusters of $ZnO_2$ (Fig. 3A) [24]. In this method, the nucleation and growth of NPs are separated into two parts: firstly, at the overheated zone, nanochemistry occurs and the formed NPs assembled as nanoclusters; secondly, these nanoclusters will erupt into colder regions for further growth. Such a tendency could be harnessed to regulate the size of NPs. Specifically, zinc acetate solution was mixed with $H_2O_2$ and placed in a Petri dish, and then suddenly introduced to a superheated plate (300 °C), the solution can be observed to change from colorless to milky white, $ZnO_2$ NPs are thus formed.

All in all, the size of $ZnO_2$ NPs prepared by this method could be adjusted by changing the concentration of zinc acetate (Fig. 3B). Its synthesis path is very simple and takes a short time, and the NPs prepared are very uniform and excellent monodispersity, which is suitable
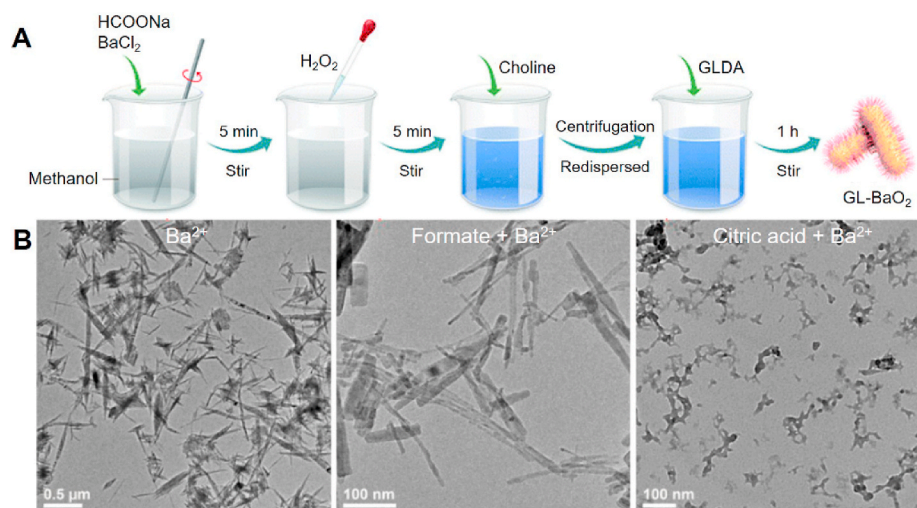
**Fig. 2.** (A) Schematic diagram of the preparation procedure of GL-BaO$_2$ NPs. (B) TEM images of the formed BaO$_2$ particles with different precursors, including Ba$^{2+}$, formate + Ba$^{2+}$, and citric acid + Ba$^{2+}$. Reproduced with permission from Ref. [21]. Copyright 2019, Royal Society of Chemistry.
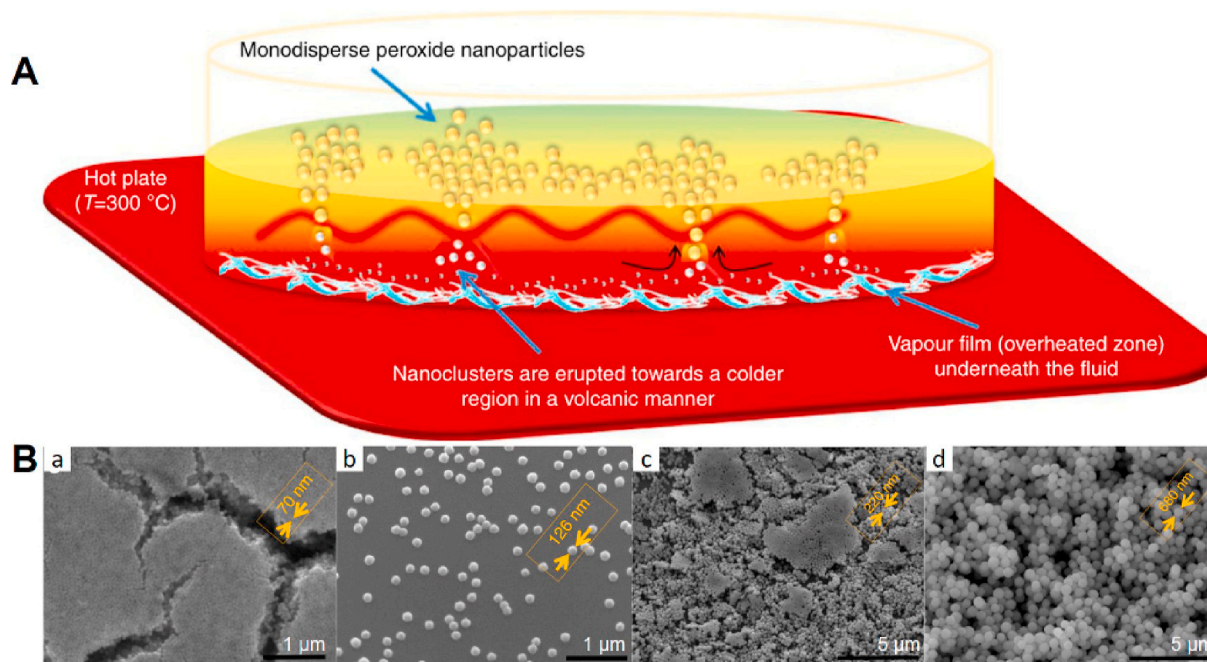


**Fig. 3.** (A) Scheme of Leidenfrost dynamic chemistry approach. (B) SEM images of the ZnO$_2$ NPs with different sizes synthesized by regulating the concentration of zinc acetate: a) 70 mM, ~70 nm; b) 50 mM, ~126 nm; c) 20 mM, ~220 nm; d) 5 mM, ~680 nm. Reproduced with permission from Ref. [24]. Copyright 2017, Nature Publishing Group.

for mass production. On the basis of ZnO$_2$, more MO$_2$ nanomaterials can be prepared.

### 2.3. Reversed-phase microemulsion method

As a new preparation method, reversed-phase microemulsion method has simple equipment and technology. It can provide a nano-scale microreactor and control the appearance of NPs more precisely. The prepared NPs have the advantages of small particle size, good dispersion, and no impurities, etc. Which is a promising preparation method and MO$_2$ can also be prepared by reversed microemulsion method.

CO-520 is always used as a nonionic surfactant in reversed-phase microemulsion. There had a report to synthesize MgO$_2$ nanosheets

[39]. Cyclohexane and CO-520 were added into MgCl$_2$ solution to create a microemulsion system. After 30 min stirring, ammonium hydroxide was rapidly injected to forming the Mg(OH)$_2$ and keep stirring for 30 min. Then H$_2$O$_2$ was added to control the reaction process and anhydrous ethanol was used to destroy the reverse microemulsion system to obtain the MgO$_2$ nanosheets. Similarly, Xiang et al. fabricated CaO$_2$ nanoparticle and simultaneous incorporation of cisplatin and coating with negatively charged phospholipid through reverse microemulsion method [25].

In the reaction of microemulsion, the size of NPs can be adjusted by adjusting the water content and pH of reversed micelles. The organic solvent phase and surfactant membrane in the microemulsion system effectively isolated the precipitation particles and improved the dispersibility of the particles. Some chemotherapeutic drugs can also be

directly added into the microemulsion system to prepare NPs and carry out drug loading at the same time. Thus, reversed-phase microemulsion is a convenient and rapid method for the preparation of $MO_2$.

## 2.4. Gas diffusion method

The gas diffusion method is often used as the preferred method for studying biomimetic synthesis of calcium carbonate ($CaCO_3$) minerals, which has the advantages of simple operation and easy observation. Deng and his colleagues designed a new synthesis approach of $CaO_2$ based on the gas diffusion synthesis of $CaCO_3$ [26]. Typically, the beaker containing the ethanol solution with $CaCl_2$ and $H_2O_2$ was covered by parafilm with a few pores, afterwards another beaker containing ammonia was placed in the same desiccator. The gas diffusion reaction will lasts for 2 h at 35 °C, the preparation of $CaO_2$ was completed. In fact, it is also an extension of the hydrolytic precipitation process described above.

This reaction is mild and simple, moreover, the prepared NPs presented monodispersed spherical morphology, the size was controlled below 100 nm and uniformed, it layed a foundation for the further construction of nanoplatform with it as the core.

## 2.5. Sonochemical method

Sonochemical method is a kind of "green" chemical synthesis method, the cavitation collapse of ultrasonic will produce chemical and physical effects so as to drive some reactions, the process of sonochemical synthesis is mild with improved yields and selectivities, can even replace some dangerous reagents, which gradually become a new method in the field of nanochemical synthesis [45].

Mahtab Pirouzmand and co-workers prepared $ZnO_2$ through sonochemical approach innovatively [27]. Their approach is so simple that $ZnSO_4 \cdot 7H_2O$ was dissolved in distilled water, and NaOH was added dropwise to adjust pH to 8.0. Followed by adding $H_2O_2$ and the mixture was irradiated under ultra-sound for half an hour, and then the $ZnO_2$ particles with great uniform size distribution and spherical shape were obtained. However, agglomeration of particles was observed. It remains to be explored how to adjust the particle size and improve the dispersion of NPs.

## 3. $MO_2$ based monotherapy

In recent years, $MO_2$ often be introduced as an $O_2$-generating material applied to the construction of tumor theranostics nanoplatform, which can regulate the TME to create a new work environment for those therapy whose efficacy is limited by the original TME. In addition, free metal ions can be involved in biological applications such as imaging and bone regeneration, made $MO_2$ a potential biological materials. This section will focus on $MO_2$-based monotherapy, including photodynamic therapy (PDT), chemodynamic therapy (CDT), and chemotherapy.

### 3.1. Oxidation therapy

Reactive oxygen species (ROS) including superoxide anion radical ($\cdot O_2^-$), $^1O_2$, $H_2O_2$, and $\cdot OH$ can damage lipids, proteins, and DNA, resulting in cell apoptosis and death [46]. The process of ROS levels exceeding the antioxidant capacity of cells and leading to cell death is called oxidative stress [47,48]. Oxidative stress has been widely used in tumor treatment in recent years, $MO_2$ is such a good material can lead oxidative stress in cells.

In the work of Chen, a PVP-modified $ZnO_2$ NPs was developed and doped with paramagnetic $Mn^{2+}$ ions through cation exchange method [38]. In this system, $ZnO_2$ will be decomposed into $Zn^{2+}$ and $H_2O_2$ in the weakly acidic TME. It is worth mentioning that $Zn^{2+}$ has been reported to increase the mitochondria production of ROS by inhibiting the electron transfer chain [49–51], and the release of $H_2O_2$ increases the

exogenous $H_2O_2$ to the cell. The endogenous generation combined with the exogenous release of ROS resulting in better tumor killing effect.

Bu et al. constructed transferrin-modified $MgO_2$ nanosheets (TMNSs), which have a corresponding response to the neutral acidity and low CAT activity of TME, $MgO_2$ reacts with $H^+$ to generate $H_2O_2$ rapidly and damages the structure of transferrin on the surface of the nanosheets [39]. Then, transferrin releases the trapped $Fe^{3+}$ and generates cytotoxic $\cdot OH$ through the Fenton reaction. The high concentration of $H_2O_2$ and the generated $\cdot OH$ destroyed tumor cells together, while TMNSs in weakly alkaline normal cells only generate a small amount of $H_2O_2$ that is enough to be decomposed by CAT. Thus, this nanosystem showed excellent tumor selectivity.

## 3.2. Photodynamic therapy

PDT utilizes photosensitizers (PS) to convert the local molecular oxygen into cytotoxic ROS, ROS can damage biological macromolecules and induce cell apoptosis [52,53]. However, the efficacy of PDT is extremely dependent on the $O_2$ concentration, thus the hypoxia of solid tumors has limited the efficacy of PDT [54], and the further $O_2$ consumption of PDT will aggravate the tumor's hypoxia and form a vicious circle [55]. In order to solve the above problems, $MO_2$ has been developed as an $O_2$ self-sufficient material to enhance the effect of PDT.

For instance, Zhang et al. designed a liposome-based nanoplatform for dual-stage light-driven PDT [22]. They encapsulated the hydrophilic PS (methylene blue, MB) and $CaO_2$ NPs into the aqueous cavity and hydrophobic layer, respectively. When LipoMB/$CaO_2$ reach the tumor tissue, $CaO_2$ inside liposomes would react with $H_2O$ to generate $O_2$ in the mild acidic TME, which can alleviate tumor hypoxia. Then, a short time irradiation is applied in the first stage, the singlet oxygen ($^1O_2$) would activated by MB and break the liposome by oxidized the phospholipid bilayer, $CaO_2$ is further exposed to $H_2O$ and generate more $O_2$. At last, a long time irradiation is given in the second stage, the PDT effect will improved a lot in such an $O_2$ sufficient TME. In a deeper analysis, after the alleviation of tumor hypoxia, the down-regulation of hypoxia-inducible factor-1α and vascular endothelial growth factor expression may also reduce the rate of tumor metastasis [56]. This two-stage light strategy based on $CaO_2$ is ingeniously designed to maximize the $O_2$ supply capacity of $CaO_2$. It is a nano-platform worth learning for alleviating tumor hypoxia and anti-tumor metastasis.

Similarly, hydrophobic aza-BODIPY dye (B1), oxygen-generating $CaO_2$ and hydrophilic ammonium bicarbonate ($NH_4HCO_3$) encapsulated in PEG shelled liposome to realize self-supplying $O_2$ PDT therapy also be reported [23]. In this study, $NH_4HCO_3$ acts as a thermoresponsive molecule. When the liposome system irradiated by near-infrared (NIR), B1 will cause the temperature to rise. Once the temperature reached 40 °C, $NH_4CO_3$ will be thermally decomposed to produce $CO_2$ [57], which will expand and destroy the liposomes, causing $CaO_2$ and $CO_2$ fully react to produce $O_2$ to improve the PDT effect of B1 (Fig. 4) [58]. Finally, they conducted tumor treatment experiments *in vivo* and find that enough $O_2$ generation from $CaO_2$/B1/$NH_4HCO_3$ liposome was favorable to produce $^1O_2$ in the presence of photosensitizer B1 and inhibit tumor growth even induced tumor disappearance. In addition to the above examples of light-triggered $O_2$-generation, pH seems another feasible trigger. In the work of Callan et al., $CaO_2$ particles were coated with a pH-responsive methacrylate-based co-polymer. The tertiary amine unit of the copolymer will be ionized in an acidic environment, and $CaO_2$ will therefore exposed and producing $O_2$. The TME creates a favorable conditions for the dissolution of copolymers [59]. Finally, with the help of $CaO_2$ NPs, PDT from rose bengal (a kind of PS) achieved the best effect [31].

$CaO_2$ not only generates $O_2$ itself but also provides a reaction substrate for other $O_2$-generating materials. For example, $CaO_2$ reacts with $H_2O$ to generate $H_2O_2$ (Eq (3)) which provide a raw material for manganese dioxide ($MnO_2$) for the generation of $O_2$ in a mild acid environment, Eq (4) [60]. By this way, Shi and his colleagues prepared a
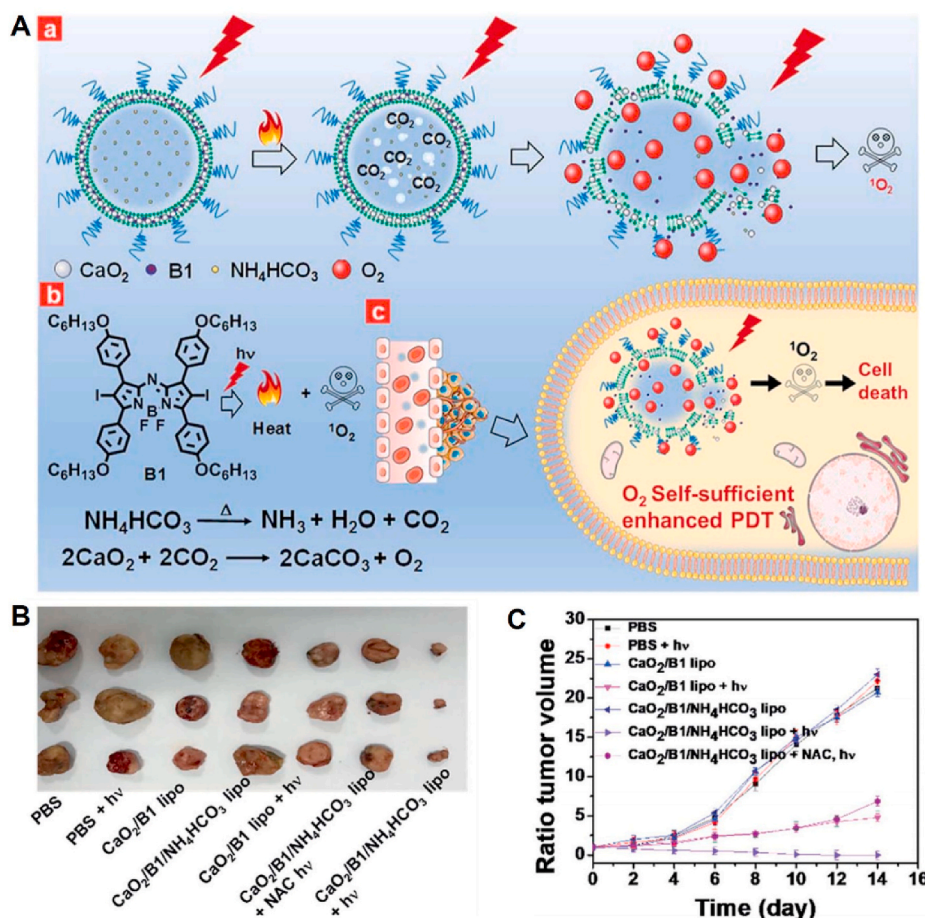
**Fig. 4.** (A) Scheme illustration of $O_2$ self-supplying enhanced PDT of $CaO_2$/B1/$NH_4HCO_3$ lipo: a) NIR-regulated generation of $O_2$ and enhancement of $^1O_2$; b) the mechanism of $O_2$ generation; c) $O_2$ self-sufficient $CaO_2$/B1/$NH_4HCO_3$ lipo enhanced PDT. (B) Photograph of tumors obtained from the mice after 14 days. (C) Tumor volume ratio of mice during the treatments. Reproduced with permission from Ref. [23]. Copyright 2019, Royal Society of Chemistry.

$CaO_2$/$MnO_2$@PDA-MB, system through $MnO_2$ nanosheet coated on the surface of $CaO_2$, in acidic TME, polydopamin (PDA) dissolution enables $Mn^{2+}$ to fully react with $H_2O_2$ produced by $CaO_2$ and generate $O_2$, further promoting the PDT effects of MB that the singlet oxygen quantum yield reached 0.18 and realized switch-control fluorescence imaging [28].

$$CaO_2 + 2H_2O \rightarrow H_2O_2 + Ca(OH)_2 \quad (3)$$

$$MnO_2 + H_2O_2 + 2H^+ \rightarrow Mn^{2+} + 2H_2O + O_2 \quad (4)$$
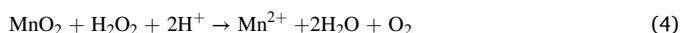
### 3.3. Chemodynamic therapy

CDT is an emerging nanotheranostic technology which catalyzes the conversion of $H_2O_2$ into ·OH through an elaborately designed Fenton nano-catalyst [61,62]. However, limited by the concentration of endogenous $H_2O_2$ in the tumor, the effect of CDT is often unsatisfactory. Since $MO_2$ can generate $H_2O_2$ in the mild acidic TME, it can be designed to enhance CDT efficacy. Moreover, the metal ions like $Cu^{2+}$, $Co^{2+}$, $Mn^{2+}$ that consisted in $MO_2$ possesses excellent Fenton catalytic activity, making $MO_2$ become a promising $H_2O_2$ self-supply CDT nanoagent [63–66].

Based on above, Jiang et al. controlled the self-assembly of $Fe_3O_4$ on the surface of HA-stabled $CaO_2$ to form $CaO_2$–$Fe_3O_4$@HA NPs. It also realizes $H_2O_2$ self-supplying CDT treatment and demonstrated a desirable performance in tumor growth inhibition rate of 69.1%, moreover, by loading Cy7 the fluorescence imaging can be combined with therapy

[29].

In another case, Chen and co-authors developed a Fenton-type copper peroxide (CP) nanodots that anchored by PVP with the aid of hydroxide ion [37]. The prepared CP nanodots could reversely decompose into $Cu^{2+}$ and $H_2O_2$ in an acidic environment, thereby realizing the $H_2O_2$ self-supplying CDT (Fig. 5A). The pH-sensitive CP nanodots were internalized by tumor by enhanced permeability and retention effects [67], and generate large amounts of ·OH through Fenton-like reaction in the acidic endo/lysosomal compartments, which can induced lysosomal membrane permeabilization-mediated tumor cell killing by lysosomal lipid peroxidation [68,69]. Finally, the authors evaluated the biological distribution of CP nanopods in U87MG tumor-bearing mice by inductively coupled plasma optical emission spectrometry found that the uptake of CP nanopods by tumors reached 5.96 ± 0.79% and showed excellent CDT anti-tumor effect with negligible weight loss (Fig. 5B–D).

### 3.4. Enhanced chemotherapy

Tumor cells have very strict mechanisms to deal with hypoxia and resist oxidation. These mechanisms are closely combined which made abnormal factors such as hypoxia, acidosis, and high glutathione (GSH) levels are simultaneously present in the TME, which promotes the drug resistance of tumor cells especially ROS-dependent drugs [70–73]. Fortunately, $MO_2$ can generates $O_2$ or by acting as a reaction substrate to reverse tumor hypoxia and providing more $O_2$ for chemo-drugs to receive enhanced chemotherapy.

Xiang et al. reported a lipid-coated $CaO_2$/cisplatin NPs which used the $O_2$ production and oxidation capabilities of $CaO_2$ at the same time to
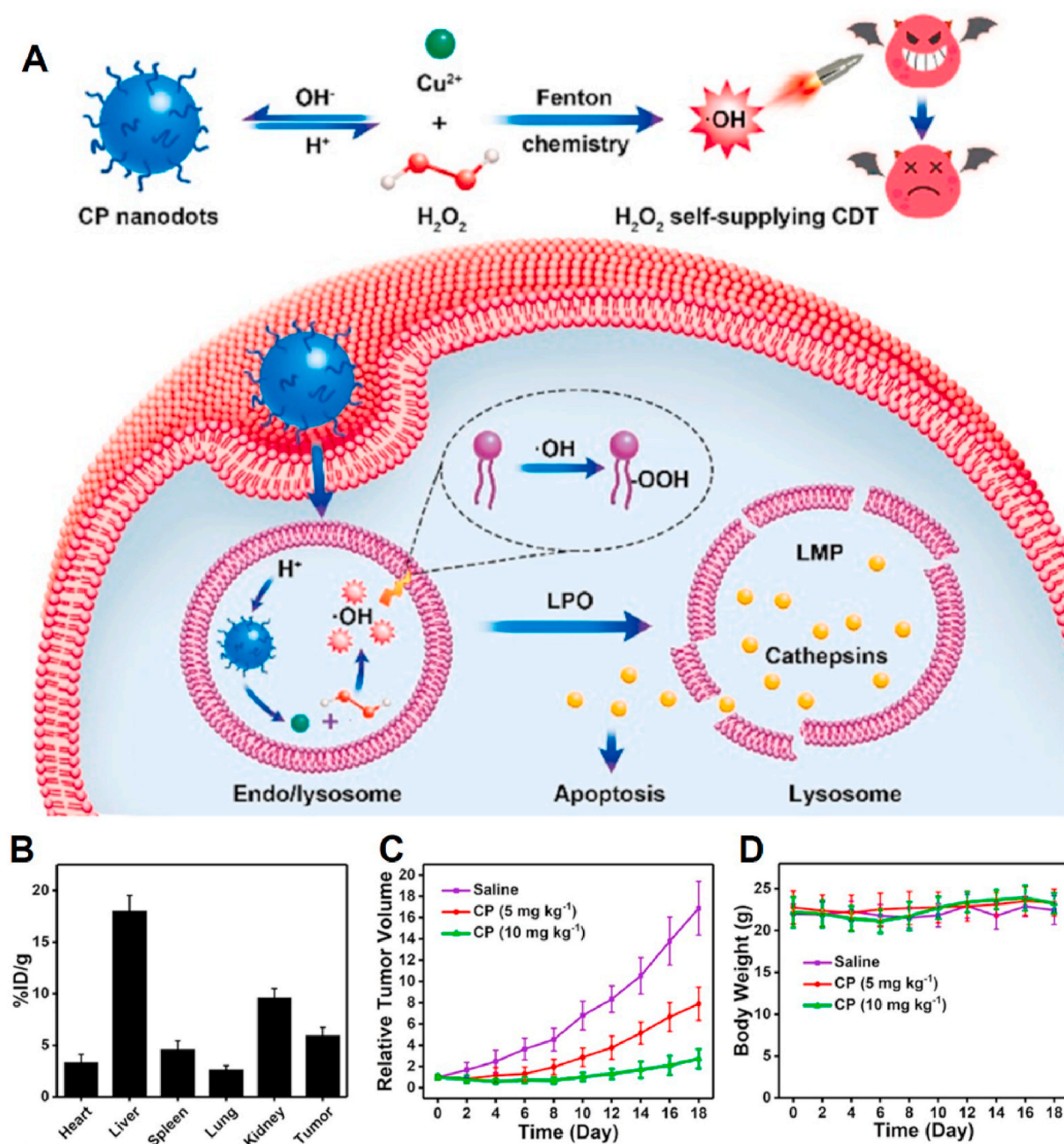
**Fig. 5.** (A) Formation of CP nanodots for $H_2O_2$ self-supplying CDT. (B) Biodistribution of Cu in major organs and tumor of U87MG tumor-bearing mice at 24 h post i. v. injection with CP nanodots. (C) Relative tumor volume and (D) variation of body weight of the mice after different treatments. Reproduced with permission from Ref. [37]. Copyright 2019, American Chemical Society.

overcome tumor hypoxia and reduce GSH levels [25]. More importantly, $CaO_2$ can significantly elevate the local pH and further accelerate GSH oxidation. After the TME was reversed, the binding of cisplatin to GSH was reduced, and the production of $O_2$ downregulated the hypoxia inducible factor 1 and resistance-associated protein 2, then the efflux pathway of cisplatin is blocked (Fig. 6A). Combined with the above process, an enhanced chemotherapy effect was achieved. As shown in Fig. 6B, fluorescent imaging showed the lipid-coated $CaO_2$/cisplatin NPs has a signal in the tumor for more than 48 h, indicating that it can achieve long circulation and efficient tumor accumulation, and the size of the tumor also showed that $CaO_2$ significantly enhanced the anti-tumor effect of cisplatin *in vivo* anti-tumor experiments intuitively (Fig. 6C and D). The work of Sung and his colleagues also proved that the $O_2$ production of $CaO_2$ also has an effect on the improvement of the

efficacy of the chemotherapy drug doxorubicin (DOX) [74]. Deng et al. used $CaO_2$, $MnO_2$ and DOX to construct $CaO_2$/DOX@$SiO_2$/DOX-$MnO_2$ nanoreactor, and proved that the drug can effectively relieve hypoxia and reverse immunosuppressive TME to enhances anti-tumor immune responses from an immunological point of view [26]. What is most worth mentioning is the drug-loading method of this nano-platform. DOX is directly added when $CaO_2$ NPs were synthesized, which can form Ca-DOX complex so that DOX can directly combine with $CaO_2$ NPs to form the $CaO_2$/DOX core and greatly improved the drug-loading efficiency.

## 4. $MO_2$ based combined therapy

The effect of monotherapy is limited, for most tumors, the treatment
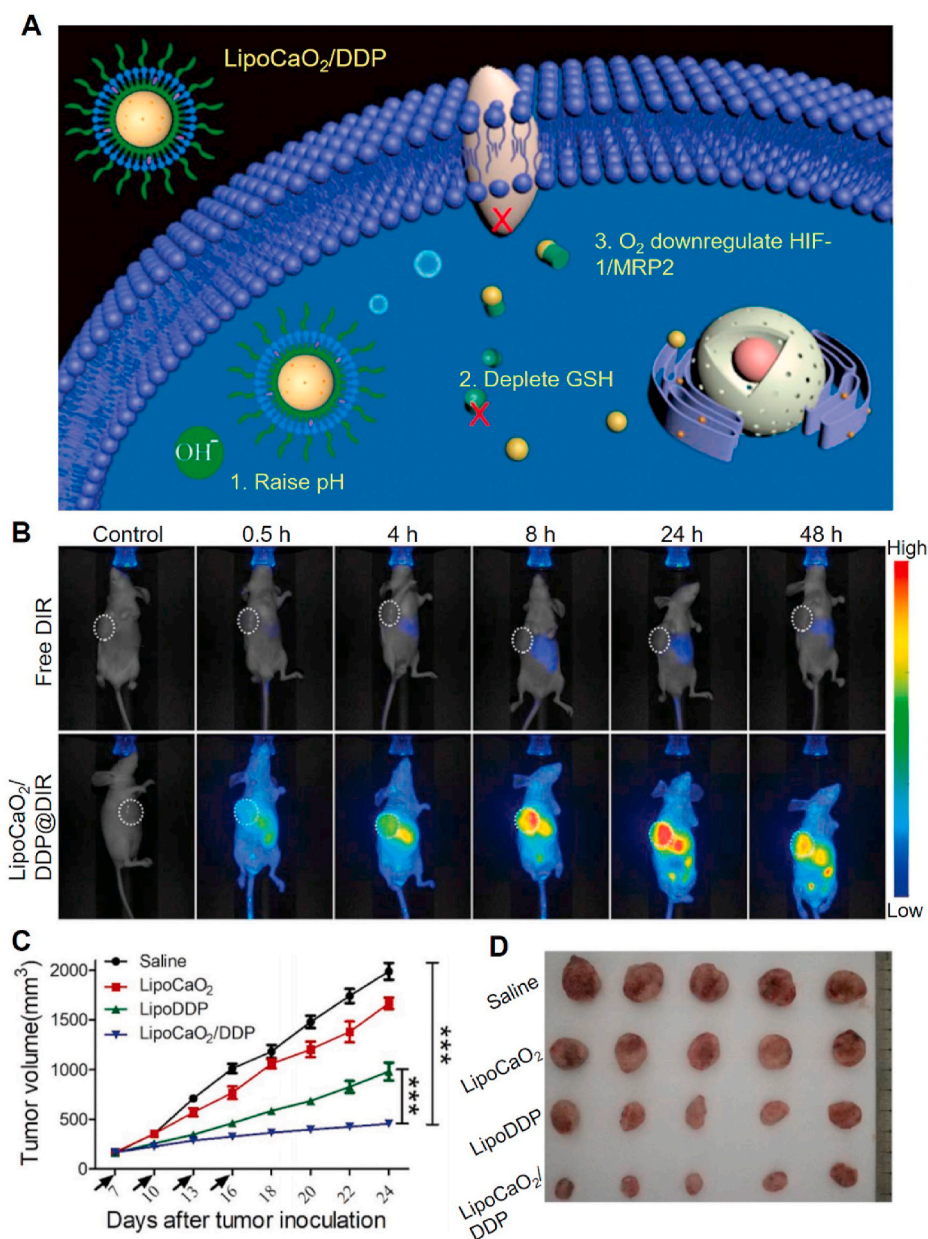
**Fig. 6.** (A) Schematic illustration of LipoCaO$_2$/DPP for comprehensive TME modulation and cisplatin efflux pathway blockade: 1) produce Ca(OH)$_2$ to raise the local pH; 2) oxidize GSH under alkaline conditions and reduce cisplatin/GSH binding; 3) generate O$_2$ for inhibition of MRP2 by HIF-1 degradation, preventing the cisplatin–GSH adduct from pumping out of cells. (B) Real-time fluorescence imaging of free fluorescein (DIR) and LipoCaO$_2$/DDP loaded DIR treated mice. (C) Tumor photographs and (D) tumor volume after different treatments. Reproduced with permission from Ref. [25]. Copyright 2019, Royal Society of Chemistry.

effect is unsatisfactory. Therefore, the combination of two or more therapeutic methods is particularly important. Each individual therapeutic agent has anti-tumor activity, and they can be built on a platform to achieve the effect of combined therapy. In addition, if the tumor killing mechanism of each therapeutic agent can complement each other, it can also realize the "1 + 1>2″ synergistic therapeutic effect [3]. After the introduction on the application of MO$_2$ to monotherapy above, combination therapies based on MO$_2$ will be discussed in this section.

### 4.1. CDT-based combination therapy

CDT can exert better curative effect by combining with other therapies [75–77]. Utilized the characteristics of CaO$_2$ that it can react with H$_2$O to generate H$_2$O$_2$ and O$_2$, Dong *et el.* constructed a H$_2$O$_2$/O$_2$ self-supplied thermoresponsive nanosystem (MSNs@CaO$_2$-ICG)@LA by using manganese silicate (MSNs) to load CaO$_2$ NPs and indocyanine green (ICG) and then modifying a layer of thermally dissolved lauric acid (LA, melting point: 44–46 °C). This nanosystem realized PDT/CDT synergistic cancer therapy and the tumors of MCF-7 bearing mice were

completely eliminated [33].

In the work of Zhang and co-authors, they built a cobalt-based metal-organic framework (ZIF-67) on the surface of CaO$_2$@DOX [15]. The slightly acid in tumor decomposed ZIF-67 and quickly released Co$^{2+}$ and DOX. The H$_2$O$_2$ produced by CaO$_2$ will be catalyzed by Co$^{2+}$ and produced highly toxic ·OH through the Fenton-like reaction, while the produced O$_2$ can improve the efficacy of DOX to enhance combined efficacy of CDT/chemotherapy. In another work, the Fe-GA/CaO$_2$@PCM NPs developed by Dong et al. used an organic phase change material (PCM) with a melting point of 46 °C as a protective layer, and co-encapsulate the hydrophilic iron-gallic acid (Fe-GA) and CaO$_2$ NPs [34]. After 808 nm laser irradiation, the temperature increase of Fe-GA causes the PCM to melt and exert the effect of photothermal therapy (PTT). H$_2$O$_2$ and Ca$^{2+}$ produced by CaO$_2$ participate in the Fe-based Fenton reaction and induce mitochondrial damage, respectively. PTT can futher accelerate the generation of ·OH. This nanoplatform can realized on-demand H$_2$O$_2$ self-supply for enhanced CDT/PTT treatment.

Moreover, MO$_2$-based materials can also be used in three dimensional (3D) printing technology. Among a multifunctional "all-in-one"

biomaterial platform, $CaO_2$ and $Fe_3O_4$ NPs were co-loaded into a 3D printing akermanite (AKT) scaffold, named AKT-$Fe_3O_4$–$CaO_2$ (Fig. 7) [32]. To put it simply, $CaO_2$ reacts with $H^+$ to produce $H_2O_2$ and $Ca^{2+}$, $H_2O_2$ was catalyzed by $Fe_3O_4$ to produce ·OH, while $Ca^{2+}$ can also be used for bone regeneration. In addition, $Fe_3O_4$ will produce hyperthermia under the action of alternating magnetic field (AMF). Thus, the scaffold with magnetic hyperthermia-synergistic $H_2O_2$ self-sufficient CDT and bone-regeneration function can be used effectively in the treatment of osteosarcoma.

### 4.2. Calcium-overload based combination therapy

Some harmful factors can cause dysfunction of calcium balance system and disorder of calcium distribution, leading to abnormal increase of intracellular calcium concentration, called calcium overload. Calcium overload can affect mitochondrial oxidative phosphorylation process, decrease the mitochondrial membrane potential, resulting in decrease of tissue ATP and activation of phospholipases and proteases in the cytoplasm, which cause irreversible cell damage [20,78]. In clinical treatment, internal calcification is frequently observed in certain tumors after radiotherapy or chemotherapy [79,80], so calcification is usually considered as a by-product of tumor treatment and it was found that calcified tumors often showed better treatment response. Given the importance role of $Ca^{2+}$ in cell proliferation, metabolism, and death, the overloading process may be a destructive factor against tumor cells, and provide alternative drug-free method for cancer therapy.

Based on the above, Bu et al. developed a calcium-based nanomedicine, the sodium hyaluronate (SH)-modified $CaO_2$ (SH–$CaO_2$), to induce intracellular calcium overloading for cancer treatment (Fig. 8A) [20]. Results revealed that $Ca^{2+}$ and $H_2O_2$ produced by $CaO_2$ caused intracellular calcium overload and oxidative stress, respectively. For the CAT down-regulated tumor cells, oxidative stress will change the function of the protein and hinder the accurate transmission of the calcium signal, thereby causing uncontrollable accumulation of $Ca^{2+}$ and inducing cell death [81]. Computer tomography (CT) imaging and von Kossa staining further showed that SH-$CaO_2$ NPs can accelerate the process of tumor calcification (Fig. 8B and C). In addition, the *in vivo* experiments also proved that SH-$CaO_2$ NPs has significant anti-tumor effect whether intratumoral injection or intravenous injection, and the anti-tumor effect of intratumoral injection is better, which caused the tumor almost disappeared during the observation period of 14 days after the injection (Fig. 8D). Similarly, the nanosystem constructed by Yin et al. with $CaO_2$ as $O_2$ source and hematoporphyrin monomethyl either as photosensitizer also combined PDT and calcium overload [82].

### 4.3. Radiation-assisted metal ion interference therapy

High Z elements have a significant effect on radiosensitization [83], but most metal-based nanomedicines are hindered in clinical application due to the biological toxicity of heavy metals. Bu and his co-authors developed a $BaO_2$-based *N,N*-bis(carboxymethyl)-L-glutamic acid tetrasodium salt (GLDA) modified nanoplatform [21]. The chelation of $Ba^{2+}$
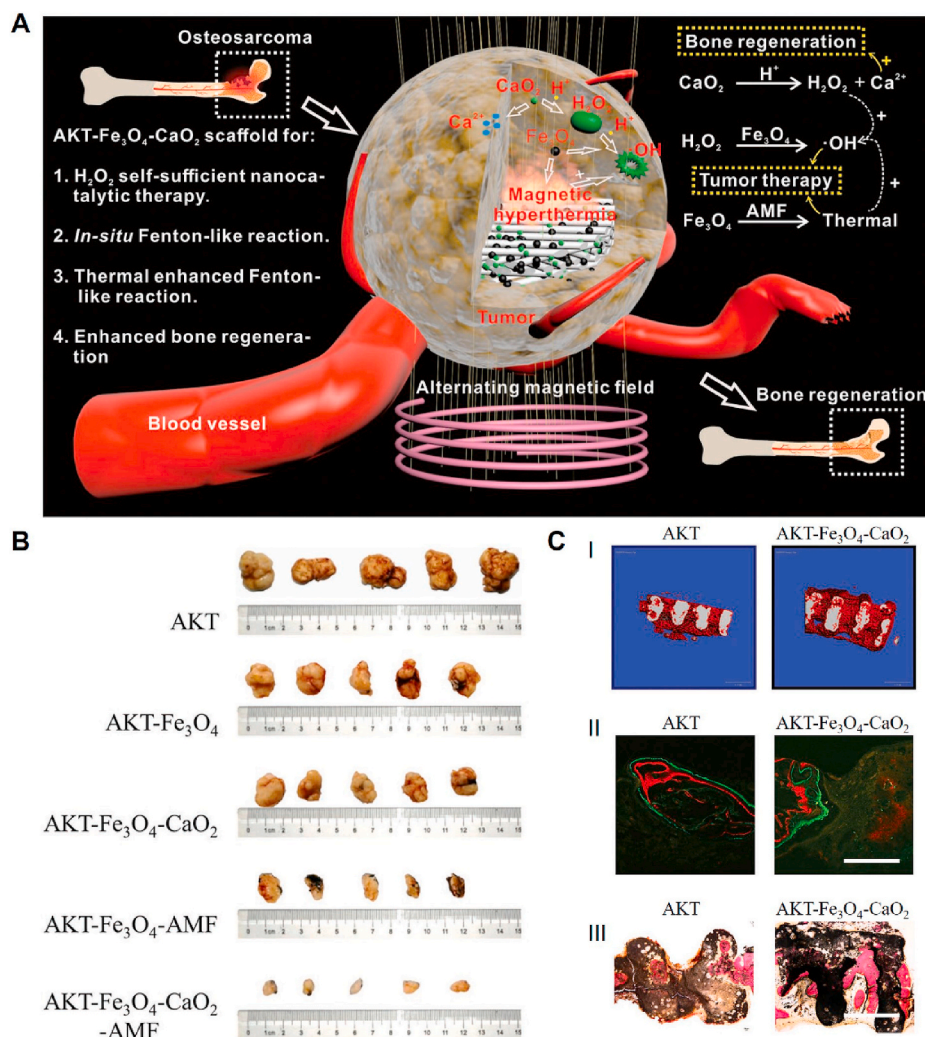


**Fig. 7.** (A) Schematic of the cancer-therapeutic performance and bone-regeneration bioactivity of AKT-$Fe_3O_4$–$CaO_2$. (B) *In vivo* anti-tumor effect. (C) *In vivo* osteogenesis capability of AKT-$Fe_3O_4$–$CaO_2$ scaffolds: I) 3D reconstruction of micro-CT images of the cranium and scaffolds (red, newborn bone tissues; white, residual scaffolds). II) CLSM images of slices from the bone defect area (yellow, newborn bone stained by tetracycline hydrochloride injected at week 2; red, newborn bone stained by Alizarin Red S injected at week 4; green, newborn bone stained by calcein injected at week 6. III) Microscopy image of VG stained slices of cranium with two defects implanted with AKT or AKT-$Fe_3O_4$–$CaO_2$ scaffolds. Scale bar, 500 μm. Reproduced with permission from Ref. [32]. Copyright 2019, Wiley-VCH. F
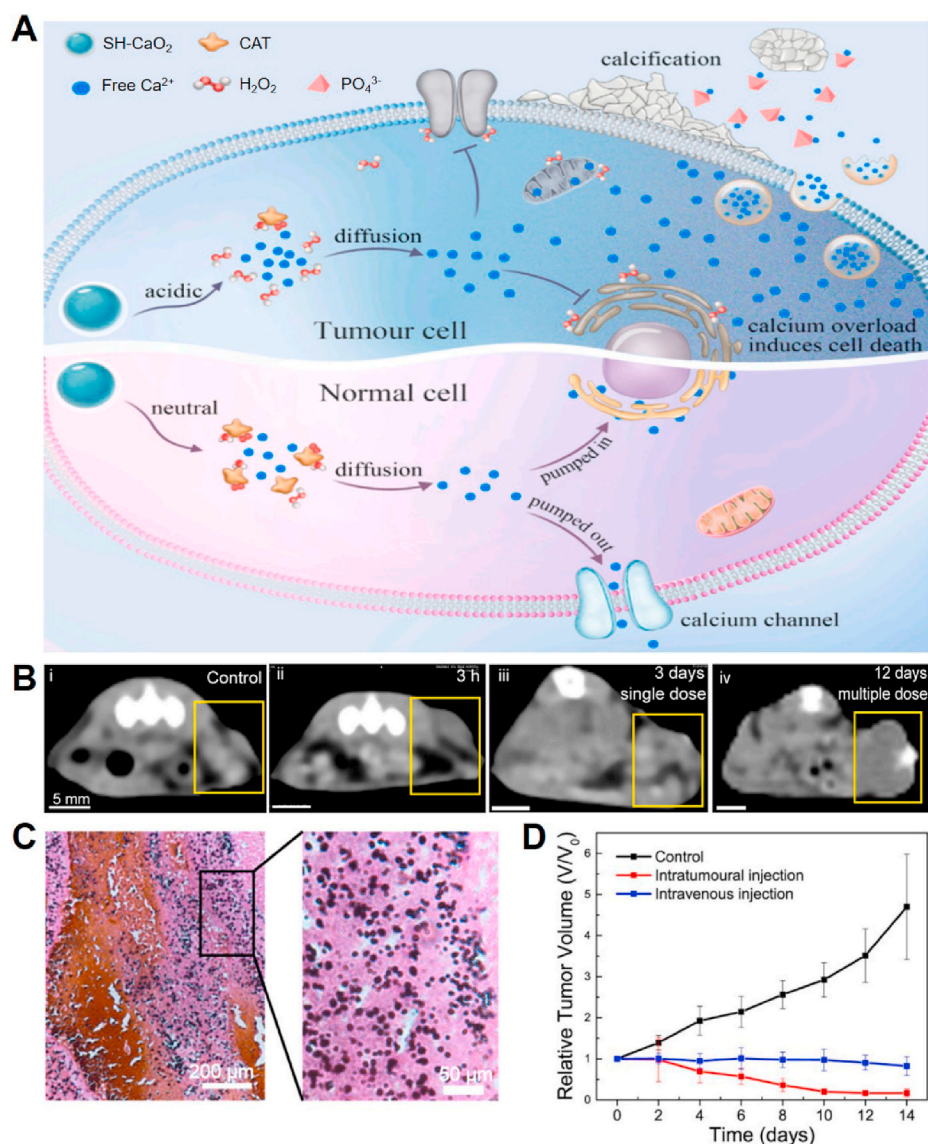
**Fig. 8.** (A) Schematic illustration of the functional pattern of SH-CaO$_2$ NPs. (B) CT images of mice after the following treatments: i) control, ii) 3 h after intratumor injection of SH-CaO$_2$ NPs, iii) 3 days after the injection of a single dose of SH-CaO$_2$ NPs for a small tumor, and iv) 12 days after the injection of multiple dose (4 times, injected every 2 days) for a larger tumor. (C) von Kossa staining of tumor tissue sections after multiple injections with SH-CaO$_2$ NPs. (D) Relative tumor volume changes during the treatments. Reproduced with permission from Ref. [20]. Copyright 2019, Elsevier.

with GLDA can reduce the toxic and side effects of the drug in normal tissues, then the $^{.}OH$ produced after X-ray radiation will destroy the chemical structure of GLDA and release Ba$^{2+}$. Benefit from this point, they proposed an ion interference therapy. The free Ba$^{2+}$ not only enhanced the radiosensitization effect but also targeted and competitively binded to potassium channels after entering the cell, then the potassium conducting pores would be blocked and the outflow of potassium ions (K$^{+}$) would be prevented [84,85], which further affect cell membrane potential and the osmotic pressure in the cell, ultimately inhibit cell proliferation and induce cell death [86,87].

## 5. Conclusions

MO$_2$ has been developed in terms of self-supplying O$_2$ and self-supplying H$_2$O$_2$, and has become a very potential therapeutic agent for tumor. Under acidic conditions, the generated H$_2$O$_2$ through MO$_2$ reacting with H$_2$O not only leads to oxidative stress, but also produce more O$_2$ by acting as a reaction substrate for substances such as CAT or MnO$_2$, so as to alleviate tumor hypoxia and reverse TME. More importantly, the characteristics of MO$_2$ can be perfectly combined with photosensitizer, enzyme, metal NPs, Fenton reagent or chemotherapy drugs, etc., which can assist and promote various treatments such as

PDT, CDT and chemotherapy. If combined multiple treatments, MO$_2$-based combination therapy will achieve more excellent anti-tumor effects.

Here, we have introduced the preparation and surface modification methods of MO$_2$-based nanomaterials and their application in tumor therapy in detail, including monotherapy and combination therapy, with emphasis on MO$_2$-based PDT, CDT, chemotherapy, oxidation therapy and ion therapy (Table 1). However, the application of MO$_2$-based nanomaterials in tumor therapy is still in the preliminary stage of research, and there are still many problems and challenges to be solved.

Firstly, morphology and size are key factors affecting the efficacy of nanomaterials, from previous studies, large NPs are more likely to retention in tumor tissue than small ones, while permeability is opposite, the smaller the size, the greater the ability to penetrate tumor tissue [88]. The size design of MO$_2$ should in accordance with the functional requirements to regulate. If MO$_2$ is used as the cargo, it is better design small size, which can not only implement efficient load but can accelerate the reaction rate of MO$_2$ in the TME. On the other side, if MO$_2$ is used as the carrier, large size may increase the rate of drug loading. In addition to particle size, morphology also plays an important role in tumor penetration. Most studies have shown that the tumor penetration ability of spherical NPs is lower than that of other shaped NPs [89]. At

present, the morphology of $MO_2$ is basically spherical, it is necessary to design $MO_2$ with other morphology to increase the tumor permeability.

Secondly, there are few types of $MO_2$ reported for tumor therapy so far, and most of the reported researches are focused on $CaO_2$-based nanomaterials. Other $MO_2$-based nanomaterials such as $MgO_2$, $BaO_2$, $ZnO_2$, $CuO_2$-based materials have not been fully developed and their biological applications are also limited, developing them by modifying them appropriately or combining them with other therapeutic agents may be a trend of future research. In the abovementioned $MO_2$, we believe that $CaO_2$ has the most clinical translation value by far. $Ca^{2+}$ is widely distributed in the body, endowing $CaO_2$ with good biocompatibility. In addition, $Ca^{2+}$ is also distributed in tumor cells, so treatment strategies such as calcium overload have universality, and $Ca^{2+}$ has the effect of accelerating osteogenesis, which can be well applied in the treatment of bone tissue related cancer such as osteosarcoma. However, the preparation and storage of $CaO_2$ even $MO_2$ are facing challenges, because of the instability, the morphology, size and dispersion of $MO_2$ are difficult to precise control, made it difficult to realize the mass production. Therefore, exploring some new methods for preparing $MO_2$ batch production is imperative, the Leidenfrost dynamic chemistry method is a good exploration [24]. For the clinical translation of $MO_2$, improve the stability of $MO_2$, extend drug life and ensure drug function is an urgent problem to be solved.

Thirdly, $MO_2$ has the potential to be used in a variety of therapeutic modalities, and its biological applications remained to be explored. In the reported studies, $MO_2$-based nanomaterials were mainly used in CDT, PDT and oxidation therapy, etc., but their application in magnetic heat, radiation, gas treatment and so on is rarely reported. Therefore, exploring the applications of $MO_2$ in a variety of therapies should be more innovative.

Fourthly, as summarized in this paper, different ions in $MO_2$ have additional functions. For example, $Ba^{2+}$ not only plays the role of radiotherapy sensitization, but also leads to cell death and inhibit proliferation through $K^+$ outflow from tissues [21]. $Ca^{2+}$ not only induces calcium overload but also enhances CT imaging [20]. When $CaO_2$ is used for the treatment of osteosarcoma, it had the ability to accelerate bone regeneration [32]. In addition to $Ba^{2+}$ and $Ca^{2+}$ ions, the functions of other ions have yet to be developed. Hence, mining the special function of ions in $MO_2$ may futher broaden its application in the field of tumor therapy, even the imaging effects attached to some ions can be used for tumor theranostics [90].

Next, hypoxia TME will greatly weaken the effect of immunotherapy, hypoxia-A2-adenosinergic tumor biology is a barrier to be overcome in immunotherapy [78]. $MO_2$ can reverse TME by self-supplying $O_2$ and suppressing hypoxia-adenosinergic signaling, further reducing the expression of hypoxia-inducible factor 1 and CD39/CD73 in T cells to reduce the immunosuppression effect of tumor TME [91]. Therefore, the mechanism of $MO_2$ in immunotherapy and its combination with other therapeutic methods remains to be further studied and developed.

Finally, the application of $MO_2$ needs to pay attention to its biosafety and long-term toxicity. Although the reported $MO_2$-based nanodrugs caused no damage to the normal tissues and organs even at a high dose of 50 mg $kg^{-1}$, the biosafety should be systematically evaluated for a longer time and on larger animal models. Moreover, cytotoxicity induced by other parts except $MO_2$ of nanodrug should also be considered. Furthermore, how to modify $MO_2$ materials to ensure its antitumor effect and biosafety remains to be solved. Although there are still many problems to be solved, $MO_2$ has brought new approaches to tumor therapy and its application in biological fields is worth developing and expanding. We hope that $MO_2$-based nanodrugs can be applied in more anti-tumor methods and bring good news to patients.

### Declaration of competing interest

The authors declare no conflict of interest.

### Acknowledgments

### Appendix A. Supplementary data

Supplementary data to this article can be found online at https://doi.org/10.1016/j.bioactmat.2021.01.026.

### References

[1] W. Chen, R. Zheng, P.D. Baade, S. Zhang, H. Zeng, F. Bray, et al., Cancer statistics in China, 2015, CA A Cancer J. Clin. 66 (2016) 115–132.

[2] F. Bray, J. Ferlay, I. Soerjomataram, R.L. Siegel, L.A. Torre, A. Jemal, Global cancer statistics 2018: GLOBOCAN estimates of incidence and mortality worldwide for 36 cancers in 185 countries, CA A Cancer J. Clin. 68 (2018) 394–424.

[3] W. Fan, B. Yung, P. Huang, X. Chen, Nanotechnology for multimodal synergistic cancer therapy, Chem. Rev. 117 (2017) 13566–13638.

[4] L.H. Fu, C. Qi, J. Lin, P. Huang, Catalytic chemistry of glucose oxidase in cancer diagnosis and treatment, Chem. Soc. Rev. 47 (2018) 6454–6472.

[5] L.H. Fu, C. Qi, Y.R. Hu, J. Lin, P. Huang, Glucose oxidase-instructed multimodal synergistic cancer therapy, Adv. Mater. 31 (2019), e1808325.

[6] D.M. Gilkes, G.L. Semenza, D. Wirtz, Hypoxia and the extracellular matrix: drivers of tumour metastasis, Nat. Rev. Canc. 14 (2014) 430–439.

[7] J.N. Liu, W. Bu, J. Shi, Chemical design and synthesis of functionalized probes for imaging and treating tumor hypoxia, Chem. Rev. 117 (2017) 6160–6224.

[8] T.W.H. Meijer, J.H.A.M. Kaanders, P.N. Span, J. Bussink, Targeting hypoxia, HIF-1, and tumor glucose metabolism to improve radiotherapy efficacy, Clin. Canc. Res. 18 (2012) 5585–5594.

[9] I.S. Turan, D. Yildiz, A. Turksoy, G. Gunaydin, E.U. Akkaya, A bifunctional photosensitizer for enhanced fractional photodynamic therapy: singlet oxygen generation in the presence and absence of light, Angew. Chem. Int. Ed. 55 (2015) 2875–2878.

[10] P.M. Petre, F.A.B. Jr, S. Tigan, J.R. Spears, Hyperbaric oxygen as a chemotherapy adjuvant in the treatment of metastatic lung tumors in a rat model, J. Thorac. Cardiovasc. Surg. 125 (2003) 85–95.

[11] C. Plafki, P. Peters, M. Almeling, W. Welslau, R. Busch, Complications and side effects of hyperbaric oxygen therapy, Aviat Space Environ. Med. 71 (2000) 119.

[12] H. Wang, Y. Chao, J. Liu, W. Zhu, G. Wang, L. Xu, Photosensitizer-crosslinked in-situ polymerization on catalase for tumor hypoxia modulation & enhanced photodynamic therapy, Biomaterials 181 (2018) 310–317.

[13] C. Shi, M. Li, Z. Zhang, Q. Yao, X. Peng, Catalase-based liposomal for reversing immunosuppressive tumor microenvironment and enhanced cancer chemo-photodynamic therapy, Biomaterials 233 (2020) 119755.

[14] T. Lin, X. Zhao, S. Zhao, H. Yu, H. Guo, $O_2$-generating $MnO_2$ nanoparticles for enhanced photodynamic therapy of bladder cancer by ameliorating hypoxia, Theranostics 8 (2018) 990–1004.

[15] S. Gao, Y. Jin, K. Ge, Z. Li, H. Liu, X. Dai, et al., Self-supply of $O_2$ and $H_2O_2$ by a nanocatalytic medicine to enhance combined chemo/chemodynamic therapy, Adv. Sci. 6 (2019) 1902137.

[16] R. Navik, L. Thirugnanasampanthan, H. Venkatesan, M. Kamruzzaman, F. Shafiq, Y. Cai, Synthesis and application of magnesium peroxide on cotton fabric for antibacterial properties, Cellulose 24 (2017) 3573–3587.

[17] M.L. Chou, J.S. Jean, C.M. Yang, Z.Y. Hseu, Y.H. Chen, H.L. Wang, et al., Inhibition of ethylenediaminetetraacetic acid ferric sodium salt (EDTA-Fe) and calcium peroxide ($CaO_2$) on arsenic uptake by vegetables in arsenic-rich agricultural soil, J. Geochem. Explor. 163 (2016) 19–27.

[18] D.P. Cassidy, R.L. Irvine, Use of calcium peroxide to provide oxygen for contaminant biodegradation in a saturated soil, J. Hazard Mater. 69 (1999) 25–39.

[19] H.J. Bae, D.C. Cho, S.H. Kwon, Enviro-chemical changes in shoreline sediment by $MgO_2$ for enhancement of indigenous microbial activity, J. Environ. Sci. Int. 19 (2010) 617–625.

[20] M. Zhang, R. Song, Y. Liu, Z. Yi, X. Meng, J. Zhang, et al., Calcium-overload-mediated tumor therapy by calcium peroxide nanoparticles, Inside Chem. 5 (2019) 2171–2182.

[21] M. Zhang, B. Shen, R. Song, H. Wang, B. Lv, X. Meng, et al., Radiation-assisted metal ion interference tumor therapy by barium peroxide-based nanoparticles, Mater. Horiz. 6 (2019) 1034–1040.

[22] L.H. Liu, Y.H. Zhang, W.X. Qiu, L. Zhang, F. Gao, B. Li, et al., Dual-stage light amplified photodynamic therapy against hypoxic tumor based on an $O_2$ self-sufficient nanoplatform, Small 13 (2017) 1701621.

[23] Q. Yu, T. Huang, C. Liu, M. Zhao, M. Xie, G. Li, et al., Oxygen self-sufficient NIR-activatable liposomes for tumor hypoxia regulation and photodynamic therapy, Chem. Sci. 10 (2019) 9091–9098.

[24] M. Elbahri, R. Abdelaziz, D. Disci-Zayed, S. Homaeigohar, J. Sosna, D. Adam, et al., Underwater Leidenfrost nanochemistry for creation of size-tailored zinc peroxide cancer nanotherapeutics, Nat. Commun. 8 (2017) 15319.

[25] C. He, X. Zhang, R. Yan, P. Zhao, Y. Chen, M. Li, et al., Enhancement of cisplatin efficacy by lipid-CaO$_2$ nanocarrier-mediated comprehensive modulation of the tumor microenvironment, Biomater. Sci. 7 (2019) 4260–4272.

[26] J. Wang, L. Fang, P. Li, L. Ma, W. Na, C. Cheng, et al., Inorganic nanozyme with combined self-oxygenation/degradable capabilities for sensitized cancer immunochemotherapy, Nano-Micro Lett. 11 (2019) 74.

[27] M. Pirouzmand, P.S. Sani, Z. Ghasemi, S. Azizi, Citric acid-crosslinked beta-cyclodextrin supported zinc peroxide as a biocompatible H$_2$O$_2$ scavenger, J. Biol. Inorg. Chem. 25 (2020) 411–417.

[28] C. Ji, Z. Lu, Y. Xu, B. Shen, S. Yu, D. Shi, Self-production of oxygen system CaO$_2$/MnO$_2$@PDA-MB for the photodynamic therapy research and switch-control tumor cell imaging, J. Biomed. Mater. Res. B 106 (2018) 2544–2552.

[29] Y. Han, J. Ouyang, Y. Li, F. Wang, J.H. Jiang, Engineering H$_2$O$_2$ self-supplying nanotheranostic platform for targeted and imaging-guided chemodynamic therapy, ACS Appl. Mater. Interfaces 12 (2020) 288–297.

[30] Y. Hu, X. Wang, P. Zhao, H. Wang, W. Gu, L. Ye, Nanozyme-catalyzed oxygen release from calcium peroxide nanoparticles for accelerated hypoxia relief and image-guided super-efficient photodynamic therapy, Biomater. Sci. 8 (2020) 2931–2938.

[31] Y. Sheng, H. Nesbitt, B. Callan, M.A. Taylor, M. Love, A.P. Mchale, et al., Oxygen generating nanoparticles for improved photodynamic therapy of hypoxic tumours, J. Contr. Release 264 (2017) 333–340.

[32] S. Dong, Y. Chen, L. Yu, K. Lin, X. Wang, Magnetic hyperthermia–synergistic H$_2$O$_2$ self-sufficient catalytic suppression of osteosarcoma with enhanced bone-regeneration bioactivity by 3D-printing composite scaffolds, Adv. Funct. Mater. 30 (2019) 1907071.

[33] C. Liu, Y. Cao, Y. Cheng, D. Wang, T. Xu, L. Su, et al., An open source and reduce expenditure ROS generation strategy for chemodynamic/photodynamic synergistic therapy, Nat. Commun. 11 (2020) 1735.

[34] S.C. Zhang, C.Y. Cao, X.Y. Lv, H.M. Dai, Z.H. Zhong, C. Liang, et al., A H$_2$O$_2$ self-sufficient nanoplatform with domino effects for thermal-responsive enhanced chemodynamic therapy, Chem. Sci. 11 (2020) 1926–1934.

[35] S. Gao, X. Lu, P. Zhu, H. Lin, L. Yu, H. Yao, et al., Self-evolved hydrogen peroxide boosts photothermal-promoted tumor-specific nanocatalytic therapy, J. Mater. Chem. B 7 (2019) 3599–3609.

[36] J.S. Park, Y.J. Song, Y.G. Lim, K. Park, Facile fabrication of oxygen-releasing tannylated calcium peroxide nanoparticles, Materials 13 (2020) 3864.

[37] L.S. Lin, T. Huang, J. Song, X.Y. Ou, Z. Wang, H. Deng, et al., Synthesis of copper peroxide nanodots for H$_2$O$_2$ self-supplying chemodynamic therapy, J. Am. Chem. Soc. 141 (2019) 9937–9945.

[38] L.S. Lin, J.F. Wang, J. Song, Y. Liu, G. Zhu, Y. Dai, et al., Cooperation of endogenous and exogenous reactive oxygen species induced by zinc peroxide nanoparticles to enhance oxidative stress-based cancer therapy, Theranostics 9 (2019) 7200–7209.

[39] Z.M. Tang, Y.Y. Liu, D.L. Ni, J.J. Zhou, M. Zhang, P.R. Zhao, et al., Biodegradable nanoprodrugs: "delivering" ROS to cancer cells for molecular dynamic therapy, Adv. Mater. 32 (2020), e1904011.

[40] J. Khodaveisi, H. Banejad, A. Afkhami, E. Olyaie, S. Lashgari, R. Dashti, Synthesis of calcium peroxide nanoparticles as an innovative reagent for *in situ* chemical oxidation, J. Hazard Mater. 192 (2011) 1437–1440.

[41] S. Shen, M. Mamat, S. Zhang, J. Cao, Z.D. Hood, L. Figueroa-Cosme, et al., Synthesis of CaO$_2$ nanocrystals and their spherical aggregates with uniform sizes for use as a biodegradable bacteriostatic agent, Small 15 (2019), e1902118.

[42] W.M. Garmett, Leidenfrost' phenomenon, Nature 17 (1878) 466.

[43] B.S. Gottfried, K.J. Bell, Film boiling of spheroidal droplets. Leidenfrost phenomenon, Ind. Eng. Chem. Fund. 5 (1966) 561–568.

[44] R.W. Henley, B.R. Berger, Self-ordering and complexity in epizonal mineral deposits, Annu. Rev. Earth Planet Sci. 28 (2000) 669–719.

[45] P. Cintas, J.L. Luche, Green chemistry. The sonochemical approach, Green Chem. 1 (1999) 115–125.

[46] B. Yang, Y. Chen, J. Shi, Reactive oxygen species (ROS)-Based nanomedicine, Chem. Rev. 119 (2019) 4881–4985.

[47] M.P. Murphy, How mitochondria produce reactive oxygen species, Biochem. J. 417 (2009) 1–13.

[48] K. Apel, H. Hirt, Reactive oxygen species: metabolism, oxidative stress, and signal transduction, Annu. Rev. Plant Biol. 55 (2004) 373–399.

[49] R.S. Balaban, S. Nemoto, T. Finkel, Mitochondria, oxidants, and aging, Cell 120 (2005) 483–495.

[50] V. Kolenko, E. Teper, A. Kutikov, R. Uzzo, Zinc and zinc transporters in prostate carcinogenesis, Nat. Rev. Urol. 10 (2013) 219–226.

[51] R.B. Franklin, L.C. Costello, Zinc as an anti-tumor agent in prostate cancer and in other cancers, Arch. Biochem. Biophys. 463 (2007) 211–217.

[52] W. Fan, P. Huang, X. Chen, Overcoming the Achilles' heel of photodynamic therapy, Chem. Soc. Rev. 45 (2016) 6488–6519.

[53] Z. Zhou, J. Song, L. Nie, X. Chen, Reactive oxygen species generating systems meeting challenges of photodynamic cancer therapy, Chem. Soc. Rev. 45 (2016) 6597–6626.

[54] A.L. Harris, Hypoxia - a key regulatory factor in tumour growth, Nat. Rev. Canc. 2 (2002) 38–47.

[55] V.H. Fingar, The role of microvascular damage in photodynamic therapy: the effect of treatment on vessel constriction, permeability, and leukocyte adhesion, Canc. Res. 52 (1992) 4914–4921.

[56] A.M. Shannon, D.J. Bouchier-Hayes, C.M. Condron, D. Toomey, Tumour hypoxia, chemotherapeutic resistance and hypoxia-related therapies, Canc. Treat Rev. 29 (2003) 297–307.

[57] A. Boddien, F. Gartner, C. Federsel, P. Sponholz, D. Mellmann, R. Jackstell, et al., CO$_2$ -"neutral" hydrogen storage based on bicarbonates and formates, Angew. Chem. Int. Ed. 50 (2011) 6411–6414.

[58] M. Zhao, Y. Xu, M. Xie, L. Zou, Z. Wang, S. Liu, et al., Halogenated Aza-BODIPY for imaging-guided synergistic photodynamic and photothermal tumor therapy, Adv. Healthc. Mater. 7 (2018) 1800606.

[59] J.S. Fang, R.D. Gillies, R.A. Gatenby, Adaptation to hypoxia and acidosis in carcinogenesis and tumor progression, Semin. Canc. Biol. 18 (2008) 330–337.

[60] J. Yuan, Y. Cen, X.J. Kong, S. Wu, X. Chu, MnO$_2$-nanosheet-modified upconversion nanosystem for sensitive turn-on fluorescence detection of H$_2$O$_2$ and glucose in blood, ACS Appl. Mater. Interfaces 7 (2015) 10548.

[61] T. Zhongmin, L. Yanyan, H. Mingyuan, B. Wenbo, Chemodynamic therapy : tumour microenvironment-mediated Fenton and Fenton-like reactions, Angew. Chem. 131 (2019), 985-968.

[62] H. Ranji-Burachaloo, P.A. Gurr, D.E. Dunstan, G.G. Qiao, Cancer treatment through nanoparticle facilitated fenton reaction, ACS Nano 12 (2018) 11819–11837.

[63] L.S. Lin, J. Song, L. Song, K. Ke, Y. Liu, Simultaneous Fenton-like ion delivery and glutathione depletion by MnO$_2$-based nanoagent to enhance chemodynamic therapy, Angew. Chem. 57 (2017) 4902–4906.

[64] W. Yuanlin, L. Zhenglin, H. Ying, L. Jing, G. Mengyu, W. Hengxiang, et al., Photothermal conversion-coordinated Fenton-like and photocatalytic reactions of Cu$_{2-x}$Se-Au Janus nanoparticles for tri-combination antitumor therapy, Biomaterials 255 (2020) 120167.

[65] J. Fernandez, P. Maruthamuthu, A. Renken, J. Kiwi, Bleaching and photobleaching of orange II within seconds by the oxone/Co$^{2+}$ reagent in Fenton-like processes, Appl. Catal. B Environ. 49 (2004) 207–215.

[66] Z. Lingling, Z. Jiulong, C. Yongkang, Z. Yuting, L. Jinfeng, Z. Jiayan, et al., MoS$_2$-ALG-Fe/GOx hydrogel with Fenton catalytic activity for combined cancer photothermal, starvation, and chemodynamic therapy, Colloids Surf., B 195 (2020) 111243.

[67] K. Maruyama, Intracellular targeting delivery of liposomal drugs to solid tumors based on EPR effects, Adv. Drug Deliv. Rev. 63 (2011) 161–169.

[68] N. Fehrenbacher, M. Jäättelä, Lysosomes as targets for cancer therapy, Canc. Res. 65 (2005) 2993–2995.

[69] Kroemer Boya, Lysosomal membrane permeabilization in cell death, Oncogene 27 (2008) 6434–6451.

[70] Q. Tan, J.K. Saggar, M. Yu, M. Wang, I.F. Tannock, Mechanisms of drug resistance related to the microenvironment of solid tumors and possible strategies to inhibit them, Canc. J. 21 (2015) 254–262.

[71] O. Tredan, C.M. Galmarini, K. Patel, I.F. Tannock, Drug resistance and the solid tumor microenvironment, J. Natl. Cancer Inst. (Bethesda) 99 (2007) 1441–1454.

[72] T. Kietzmann, A. Gorlach, Reactive oxygen species in the control of hypoxia-inducible factor-mediated gene expression, Semin. Cell Dev. Biol. 16 (2005) 474–486.

[73] W. Li, A.N. Kong, Molecular mechanisms of Nrf2-mediated antioxidant response, Mol. Carcinog. 48 (2010) 91–104.

[74] C.C. Huang, W.T. Chia, M.F. Chung, K.J. Lin, C.W. Hsiao, C. Jin, et al., An implantable depot that can generate oxygen *in situ* for overcoming hypoxia-induced resistance to anticancer drugs in chemotherapy, J. Am. Chem. Soc. 138 (2016) 5222–5225.

[75] L.H. Fu, Y.R. Hu, C. Qi, T. He, S. Jiang, C. Jiang, et al., Biodegradable manganese-doped calcium phosphate nanotheranostics for traceable cascade reaction-enhanced anti-tumor therapy, ACS Nano 13 (2019) 13985–13994.

[76] L. Zhang, S.S. Wan, C.X. Li, L. Xu, H. Cheng, X.Z. Zhang, An adenosine triphosphate-responsive autocatalytic fenton nanoparticle for tumor ablation with self-supplied H$_2$O$_2$ and acceleration of Fe(III)/Fe(II) conversion, Nano Lett. 18 (2018) 7609–7618.

[77] C. Qi, J. He, L.-H. Fu, T. He, N.T. Blum, X. Yao, et al., Tumor-specific activatable nanocarriers with gas-generation and signal amplification capabilities for tumor theranostics, ACS Nano (2020), https://doi.org/10.1021/acsnano.0c09223.

[78] M.V. Sitkovsky, S. Hatfield, R. Abbott, B. Belikoff, D. Lukashev, A. Ohta, Hostile, hypoxia-A2-adenosinergic tumor biology as the next barrier to overcome for tumor immunologists, Canc. Immunol. Res. 2 (2014) 598–605.

[79] L. Pantngrag-Brown, Calcification and fibrosis in mesenteric carcinoid tumor: CT findings and pathologic correlation, Am. J. Roentgenol. 164 (1995) 387–391.

[80] D.D. Dershaw, C.S. Giess, B. Mccormick, P. Borgen, L. Liberman, A.F. Abramson, et al., Patterns of mammographically detected calcifications after breast-conserving therapy associated with tumor recurrence, Cancer 79 (2015) 1355–1361.

[81] S. Orrenius, B. Zhivotovsky, P. Nicotera, Regulation of cell death: the calcium-apoptosis link, Nat. Rev. Mol. Cell Biol. 4 (2003) 552–565.

[82] X. Rui, Y. Yang, J. Wu, J. Chen, Q. Chen, R. Ren, et al., Multi-path tumor inhibition via the interactive effects between tumor microenvironment and an oxygen self-supplying delivery system for a photosensitizer, Photodiagn. Photodyn. 29 (2020) 101642.

[83] F. Lux, L. Sancey, A. Bianchi, Y. Crémillieux, S. Roux, O. Tillement, Gadolinium-based nanoparticles for theranostic MRI-radiosensitization, Nanomedicine 10 (2015) 1801–1815.

[84] J.M. Quayle, N.B. Standen, P.R. Stanfield, The voltage-dependent block of ATP-sensitive potassium channels of frog skeletal muscle by caesium and barium ions, J. Physiol. (Lond.) 405 (1988) 677–697.

[85] B.S. Bhoelan, C.H. Stevering, A.T.J. d B Van, M.A.G. d H Van, Barium toxicity and the role of the potassium inward rectifier current, Clin. Toxicol. 52 (2014) 584–593.

[86] N. Prevarskaya, R. Skryma, Y. Shuba, Ion channels and the hallmarks of cancer, Trends Mol. Med. 16 (2010) 107–121.

[87] M.S. Sinicropi, D. Amantea, A. Caruso, C. Saturnino, Chemical and biological properties of toxic metals and use of chelating agents for the pharmacological treatment of metal poisoning, Arch. Toxicol. 84 (2010) 501–520.

[88] W. Yu, R. Liu, Y. Zhou, H. Gao, Size-tunable strategies for a tumor targeted drug delivery system, ACS Cent. Sci. 6 (2020) 100–116.

[89] Q. Sun, T. Ojha, F. Kiessling, T. Lammers, Y. Shi, Enhancing tumor penetration of nanomedicines, Biomacromolecules 18 (2017) 1449–1459.

[90] H. Chen, W. Zhang, G. Zhu, J. Xie, X. Chen, Rethinking cancer nanotheranostics, Nat. Rev. Mater. 2 (2017) 17024.

[91] I. Perrot, H.A. Michaud, M. Giraudon-Paoli, S. Augier, A. Docquier, L. Gros, et al., Blocking antibodies targeting the CD39/CD73 immunosuppressive pathway unleash immune responses in combination cancer therapies, Cell, For. Rep. 27 (2019) 2411–2425.